NASA TECHNICAL TRANSLATION NASA TT F-16,111

PHOTODISSOCIATION OF CO_2 AND THE HEAT LIBERATION ASSOCIATED WITH IT IN THE UPPER ATMOSPHERES OF MARS AND VENUS

A. V. Dembovskiy, M. N. Iskov, and O. G. Lisin

Translation of "Fotodissotsiatsiya CO_2 i svyazonnoye s ney teplovydeleniye v verkhnikh atmosferakh Marsa i Venery," Academy of Sciences USSR, Institute of Space Research, Moscow, Report Pr-165, 1974, pp. 1-38

NATIONAL AERONAUTICS AND SPACE ADMINISTRATION
WASHINGTON, D.C. 20546 JANUARY 1975

STANDARD TITLE PAGE

1. Report No. NASA TT F-16,111	2. Government Accession No.	3. Recipient's Catalog No.
4. Title and Subtitle PHOTODISSOCIATION OF CO_2 AND THE HEAT LIBERATION ASSOCIATED WITH IT IN THE UPPER ATMOSPHERES OF MARS AND VENUS		5. Report Date January 1975
		6. Performing Organization Code
7. Author(s) A. V. Dembovskiy, M. N. Iskov, and O. G. Lisin		8. Performing Organization Report No.
		10. Work Unit No.
9. Performing Organization Name and Address Leo Kanner Associates Redwood City, California 94063		11. Contract or Grant No. NASw-2481
		13. Type of Report and Period Covered Translation
12. Sponsoring Agency Name and Address National Aeronautics and Space Administration, Washington, D.C. 20546		14. Sponsoring Agency Code

15. Supplementary Notes

Translation of "Fotodissotsiatsiya CO_2 i svyazonnoye s ney teplovydeleniye v verkhnyikh atmosferakh Marsa i Venery," Academy of Sciences USSR Institute of Space Research, Moscow, Report Pr-165, 1974, pp. 1-38.

16. Abstract The photodissociation rate of CO_2 in the atmospheres of Mars and Venus was calculated. Also calculated was the heat liberation and intensities of emissions associated with photodissociation. The total bulk photodissociation rate emonotonely decreases with altitude throughout the thermosphere. The role of various photodissociation channels with excitation varies with altitude. Heat liberation due to photodissociation in the lower thermosphere (at altitudes below approximately 115 km in Mars and 140 km in Venus) is greater than due to photodissociation, and even though less in the upper thermosphere, still represents a considerable proportion of the latter. The effectiveness of heat liberation (fraction of energy of absorbed photons converted to heat) varies from 0.3 in the lower thermosphere to 0.2 at roughly 200 km in Mars and Venus and continues to decrease at greater altitudes. The photodissociation rate and specific heat liberation were obtained as universal functions (suitable for both planets) of the number of molecules along photon path.

17. Key Words (Selected by Author(s))	18. Distribution Statement
	Unclassified - Unlimited

19. Security Classif. (of this report)	20. Security Classif. (of this page)	21. No. of Pages	22. Price
Unclassified	Unclassified	32	

PRECEDING PAGE BLANK NOT FILMED

NASA-HQ

PHOTODISSOCIATION OF CO_2 AND THE HEAT LIBERATION ASSOCIATED WITH IT IN THE UPPER ATMOSPHERES OF MARS AND VENUS

A. V. Dembovskiy, M. N. Iskov, and O. G. Lisin

/4*

Photodissociation of CO_2 under the effect of ultraviolet solar radiation materially affects the composition and thermal conditions in the upper atmospheres of Mars and Venus. In several studies it was found that the predominance of CO_2 over much of the thermosphere, when there is a high photodissociation rate and a low rate of association of CO and O, indicates the important role of transport processes /1-6/. However, simplifications made in these studies (and especially, in the estimates of the efficiency of heat liberation) /4, 7, 8/ point to the necessity of more exact calculations for constructing a representative theoretical model of the thermosphere.

In this paper the photodissociation rate of CO_2 in the thermospheres of Mars and Venus is calculated with allowance for the contributions made by different channels of dissociation with excitation. In addition, the value of heat liberation associated with photodissociation is calculated. Finally, the intensity of several emissions resulting from photodissociation with excitation is calculated.

1. Main Channels of CO_2 Dissociation

By absorbing solar ultraviolet photons, CO_2 molecules dissociate, and depending on photon energy, various electron states of the dissociation products are excited:

$$CO_2 + h\nu \rightarrow CO^* + O^* \quad (1)$$

* Numbers in the margin indicate pagination in the foreign text.

Dissociation channels that are essential for the problem under study and the corresponding threshold wavelengths $\lambda_{max}^{(j)}$ are given in Table 1. /5

TABLE 1

Channel number	Reaction products	$\lambda_{max}^{(j)}$ (Å)
1.	$CO(X^1\Sigma^+) + O(^3P)$	2274
2.	$CO(X^1\Sigma^+) + O(^1D)$	1670
3.	$CO(X^1\Sigma^+) + O(^1S)$	1286
4.	$CO(a^3\Pi) + O(^3P)$	1087
5.	$CO(a'^3\Sigma^+) + O(^3P)$	1007
6.	$CO(d^3\Delta_i) + O(^3P)$	956
7.	$CO(e^3\Sigma^-) + O(^3P)$	929
8.	$CO(e^3\Sigma^-) + O(^1D)$	809
9.	$CO(e^3\Sigma^-) + O(^1S)$	707

The first three channels correspond to the formation of CO_2 molecules in the ground electronic state $CO(X^1\Sigma^+)$, and the O atoms are formed successively in the ground state $O(^3P)$ and the excited states $O(^1D)$ and $O(^4S)$. The energy of these metastable states (Einstein coefficients $A_{O(^1D \rightarrow ^3P)} = 0.0083\ sec^{-1}$, $A_{O(^1S \rightarrow ^1D)} = 1.35\ sec^{-1}$, $A_{O(^2S \rightarrow ^3P)} = 0.0824\ sec^{-1}$) can only be de-excited:

$$O(^1D) \rightarrow O(^3P) + h\nu \quad (\lambda = 6300\text{Å}), \tag{2}$$
$$O(^1S) \rightarrow O(^1D) + h\nu \quad (\lambda = 5577\text{Å}), \tag{3}$$
$$O(^1S) \rightarrow O(^3P) + h\nu \quad (\lambda = 2972\text{Å}), \tag{4}$$

or else are transformed to heat due to shock de-activation: /6

$$O(^1D, ^1S) + M \rightarrow O(^3P) + M + E_{kin}, \quad (5)$$

where M is the de-activating particle. In the thermospheres of Mars and Venus, de-activation proceeds mainly during collisions with CO_2 molecules. The coefficients of shock de-activation are $K_{O(^1D)} = 2.1 \cdot 10^{-10}$ cm^3/sec and $K_{O(^1S)} = 2.5 \cdot 10^{-4}$ cm^3/sec /9-11/.

The state of $CO(a^3\Pi)$ formed in channels No. 4 and No. 5 is also metastable, however its radiation lifetime is so short ($\tau_P = 7.5 \cdot 10^{-3}$ sec), so that its energy is virtually entirely de-excited, yielding a system of Cameron bands. The energy of the states $CO(a^{13}\Sigma^+, d^3\Delta_i, e^3\Sigma^-)$ formed in channels Nos. 5-9 is de-excited during permitted transitions to the state $CO(a^3\Pi)$.

It should be noted that beginning approximately with the ionization threshold CO_2 (λ = 899 Å), the number of possible dissociative channels becomes considerably greater than indicated in Table 1. We will see below that the contribution made by the shortwave spectral region ($\lambda \lesssim 1000$ Å) to the unknown functions is small, therefore the restriction to these channels is wholly acceptable.

2. Formulas for Calculating Photodissociation and Heat Liberation

A quantitative description of these processes can be carried out as follows /12,13/. The total photodissociation rate P_D (number of dissociation acts per cubic centimeter per second is composed of the rates of photodissociation in the listed channels $P_D^{(j)}$ and is expressed by the formula:

$$P_D(z) = \sum_j P_D^{(j)}(z) = n(z) \sum_j \int_0^{\lambda_{max}^{(j)}} \sigma_D^{(j)}(\lambda) \frac{F(\lambda, z)}{h\nu} d\lambda = n(z) \int_0^{\lambda_{max}^{(1)}} \sigma_D(\lambda) \frac{F}{h\nu} d\lambda, \quad (6)$$

where z is altitude, n is CO_2 concentration, $\delta_D^{(j)}$ is the dissociation cross-section in the j-th channel, δ_D is the total dissociation cross-section, $h\nu$ is the energy of absorbed photons (erg), $\lambda_{max}^{(j)}$ is the threshold wavelength for the j-th channel, $F(\lambda, z)$ is the spectral density of the solar radiation flux (erg/cm^2·sec·Å) at altitude z associated with flux density at the atmospheric boundary $F_\infty(\lambda)$ by the relation; /7

$$F(\lambda,z)=F_\infty(\lambda)\exp\{-\delta(\lambda)n(z)H(z)Ch(\chi,z)\}, \quad (7)$$

which is a consequence of the Bouguer-Lambert-Beer law of radiation absorption and the fact that $n(z)$ is defined by the barometric formula; here $\delta(\lambda)$ is the total cross-section of CO_2 absorption, H is the scale of CO_2 altitude, $H = \frac{R_o T}{Mg}$, R_o is the universal gas constant, T is temperature, M is molecular weight of CO_2, g is the acceleration due to gravity; $Ch(\chi, z)$ is the Chapman function, that takes into account the curvature of the atmospheric layers (when $\chi < 70^\circ$, $Ch(\chi, z) \simeq \sec\chi$).

The energy of photons absorbed per cubic centimeter per second is obviously

$$Q_g(z)=n(z)\sum_j\int_0^{\lambda_{max}^{(j)}}\sigma_D^{(j)}(\lambda)F(\lambda,z)d\lambda. \quad (8)$$

Since not all the energy of the absorbed photons is transformed into heat, to describe the rate of heat liberation Q_{ST} (the heat source in the energy balance equation), let us introduce the spectral efficiency of heat liberation in the j-th channel $\epsilon_j(\lambda, z)$, that is, the fraction of energy of the absorbed photon transformed into heat in the channel. Thus, Q_{ST} can be expressed as:

$$Q_{ST}(z)=\sum_j Q_{ST}^{(j)}(z)=n(z)\sum_j\int_0^{\lambda_{max}^{(j)}}\varepsilon_j(\lambda,z)\sigma_D^{(j)}F(\lambda,z)d\lambda \quad (9)$$

The integrated (with respect to spectrum) efficiency of heat liberation in this channel is defined as /8

$$\varepsilon_j(z) = \frac{Q_{ST}^{(j)}(z)}{Q_S(z)}. \qquad (10)$$

And the total efficiency of heat liberation at the given altitude is:

$$\varepsilon(z) = \sum_j \varepsilon_j(z) = \frac{Q_{ST}(z)}{Q_S(z)}. \qquad (11)$$

Let us also introduce the dissociation rate per particle:

$$\beta_D(z) = \frac{P_D(z)}{n(z)} \qquad (12)$$

and the specific rate of heat liberation (erg/g·sec)

$$q_{ST}(z) = \frac{Q_{ST}(z)}{\rho(z)} = \frac{Q_{ST}(z)}{m \cdot n(z)}, \qquad (13)$$

where ρ is the density and m is the mass of the CO_2 molecule. As we will see below, the desired functions P_D, q_{ST}, and ϵ depend on the model basically in terms of the total number of particles along the photon path N = nHCh(χ, Z), which enables us to plot universal functions suitable for use when calculating atmospheric models.

In order to obtain an expression for $\epsilon_j(\lambda, Z)$ let us consider that the photon energy can be transformed into heat in two ways: first, part of the excess photon energy above the dissociation energy and the excitation energy is converted into kinetic energy of the particles formed and then, upon their collision with surrounding particles, is converted into thermal energy; secondly, the energy of the metastable excited state can be transformed into heat upon shock de-activation [12].

Let us represent the contribution to ϵ_j by means of the first an and second pathways by, respectively, ϵ_j^I and ϵ_j^{II}. Thus,

$$\varepsilon_j(\lambda, z) = \varepsilon_j^I(\lambda) \cdot \varepsilon_j^I(\lambda, z). \quad (14)$$

Obviously, ϵ_j^I can be expressed in the form /9

$$\varepsilon_j^I = \frac{h\nu - E_D - W_j}{h\nu} \varphi_j(\lambda) = \left(1 - \frac{E_j}{h\nu}\right)\varphi_j(\lambda) = \left(1 - \frac{\lambda}{\lambda_{max}^{(j)}}\right)\varphi_j(\lambda), \quad (15)$$

where E_D is the energy of dissociation (E_D = 5.45 ev), E_j and $\lambda_{max}^{(j)}$ is the threshold energy ($E_j = E_D + W_j$) and the threshold wavelength of the photon for the j-th channel, respectively; W_j is the total energy of the electronic levels of O and CO excited in the j-th channel; $\phi_j(\lambda)$ is the factor of the reduction in the efficiency of heat liberation due to the excitation of the vibrational-rotational states of CO upon dissociation of CO_2 (the energy of these states is practically entirely de-excited, since the comparison of the rate of spontaneous de-excitation of CO ($X^1\Sigma^+$, $v' \gtrsim 0$) [14] and its rate of vibrational relaxation [15] shows that on both Mars and Venus the relaxation of CO can be neglected all the way to the mesopause.

In processes of dissociation and de-activation, the species O and CO with kinetic energy to approximately 2 ev are formed. Some fraction of the energy of these particles, upon collision with CO_2 molecules, can be expended in exciting the vibrational-rotational levels of CO_2 and can be de-excited. Thus far there are no direct experimental data on these processes; however, available theoretical and experimental on the collisions of CO_2 with other particles [16, 17] suggest that in the collisions with O and CO species having the indicated initial energies, of interest to us, not more than several percent of the initial energy is expended in de-excitation. Therefore in the

following we will assume that all the kinetic energy of the CO_2 dissociation products is transformed into heat.

As indicated above, only de-activation of $O(^1D)$ and $O(^1S)$ by CO_2 molecules is substantial. Therefore in the case when the atom $O(^1E)$ is formed in the j-th channel, the expression for ϵ_j^{II} can be written as /10

$$\varepsilon_j^{II}(\lambda,z)=\frac{W_{O(^1D)}}{h\nu}\cdot\frac{K_{O(^1D)}n(z)}{A_{O(^1D\to{}^3P)}+K_{O(^1D)}n(z)}\cdot\psi_{O(^1D)} \qquad (17)$$

where $A_{O(^1D \to {}^3P)}$ is the Einstein coefficient; $K_{O(^1D)}$ is the coefficient of shock de-activation of $O(^1D)$ by CO_2 molecules; $\psi_{O(^1D)}$ is the factor that takes into account the possibility of the conversion of part of the excitation-level energy into vibrational degrees of freedom of CO_2 with subsequent de-excitation. But in the case of the formation in the j-th channel of $O(^1S)$, taking into account the predominance of the transition $O(^1S) \to O(^1D)$, we can write an analogous expression for ϵ_j^{II}:

$$\varepsilon_j^{II}(\lambda,z)=\frac{W_{O(^1S)}}{h\nu}\cdot\frac{K_{O(^1S)}n(z)}{A_{O(^1S\to{}^1D)}+K_{O(^1S)}n(z)}\cdot\psi_{O(^1S)}+$$
$$+\frac{W_{O(^1D)}}{h\nu}\cdot\frac{A_{O(^1S\to{}^1D)}\psi_{O(^1S)}n(z)}{(A_{O(^1S\to{}^1D)}+K_{O(^1S)}n(z))(A_{O(^1D\to{}^3P)}+K_{O(^1D)}n(z))}\psi_{O(^1D)} \qquad (18)$$

In the general case, it must be considered that the energy expended in the dissociation of CO_2 molecules can be converted into heat in the association process in ternary collisions

(19)

yielding the heat liberation

$$Q_4=E_D\cdot\alpha\cdot n_{CO}\cdot n_O\cdot n_{CO_2}, \qquad (20)$$

where the association coefficient $\alpha \cong 10^{-35}$ cm^6/sec [18], however estimates show that for the thermospheres of Mars and Venus Q_A is many orders of magnitude lower than Q_{ST} and can always be neglected.

3. Data Used in Calculations /11

Let us examine available data and the parameters appearing in the formulas for calculation of the desired functions.

3.1. The values of $n(z)$ were calculated from the barometric formula using the given temperature profile and density of the fixed altitude. The temperature profile and cut-off density according to [2] ($T_\infty = 350^\circ$ K, n (100 km) = $5.8 \cdot 10^{11}$ cm^{-3}) were specified for the Martian thermosphere in the region $z \geqslant 100$ km; a temperature close to that of the models [19, 20] was selected for the lower altitudes. For the thermosphere of Venus, the profile $n(z)$ was calculated from the temperature profile of the model [21] ($T_\infty = 680^\circ$ K); the cut-off density n (130 km) = $1.4 \cdot 10^{12}$ cm^{-3}).

3.2. Fluxes of solar radiation $F_\infty(\lambda)$ were taken from the data of Hinteregger [22] for $\lambda < 1300$ Å and from the data of Ackerman [23] for $\lambda > 1300$ Å, reduced to the orbit of the corresponding planet.

3.3. The cross-sections of total absorption of CO_2 $\delta(\lambda)$ were taken from the data in [24, 25]. The contribution of scattering without dissociation to the total absorption of photons is small [26-30] in the spectral region that is effectively operative at the altitudes of interest to us. Therefore it can be assumed that if the photon wavelength is higher than the ionization threshold, $\delta_D(\lambda) = \delta(\lambda)$, and if less, then $\delta_D(\lambda) = \delta(\lambda) - \delta_u(\lambda)$, where $\delta_u(\lambda)$ is the photoionization cross-section of CO_2, taken from the data in [31]. At the same time, an experiment was reported by Inn [32] in which a

photolysis product yield of 0.5 was obtained for the 1400-1670 Å spectral region. Inn explained the reduction in the yield by the reradiation of photons by nondissociating CO_2 molecules. In the calculation, we will assume a unit contribution of dissociative products, however we will verify the effect of the data in [3] contradicting the rest of the experiments on our results. /12

3.4. Available experimental data and the values adopted for the relative yields of the photodissociation products $f_j(\lambda) = \delta_D^{(j)}(\lambda)/\delta_D(\lambda)$ are shown in Fig. 1. Since the measurements do not cover the entire spectral region required, a linear interpolation of the functions $f_j(\ )$ was made over several spectral intervals. Fig. 1 gives the measurement data with solid lines and with symbols, and the interpolation -- with a dashed line. Variants I and II correspond to the two experimental groups whose data differ for 800 Å $< \lambda <$ < 1037 Å $= \lambda_{max}^{(3)}$.

In the operative region of channel No. 1, 1670-2274 Å, reradiation can be the only competing process. Since it is inefficient, it can be assumed that f_1 / $1670 < \lambda < 2274$ Å / / [see c] 1. The measurements in the 1500-1600 Å range and at the lines 1470 and 1236 Å [27-30] showed that dissociation proceeds in channel No. 2 with unit efficiency. By measuring the intensity of the green line OI(5577 Å) corresponding to the forbidden transition $O(^1S \rightarrow {}^2D)$, in an experiment on the photolysis of CO_2 in the 812-1216 Å range, Lawrence determined the yield of f_3 of channel No. 3 [33] with respect to the measured cross-section of $O(^1S)$ formation to the total dissociation cross-section taken according to [24]. In another experiment [34], Lawrence measured the intensity of the Cameron bands excited upon dissociation in the 850-1090 Å spectral interval. The spectrum of this intensity, as it was found, very closely reproduces the band structure of total absorption, /13

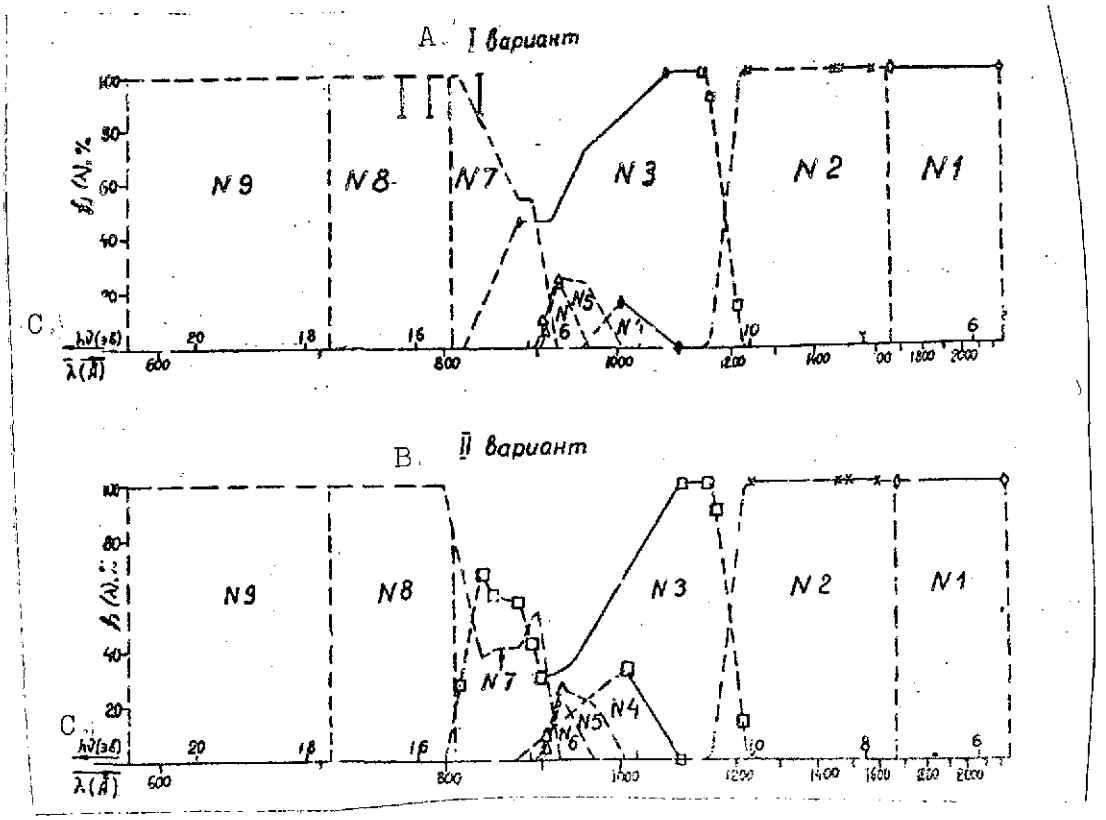

Fig. 1. Spectral dependence of relative yields of photodissociation with excitation in various channels (the channels are listed in Table 1). The solid lines and the symbols denote the experimental data, and the dashed lines denotes interpolation. ◊ - data in /26/, X - data in /27-30/, □ - data in /33/, ♦ - /34/, △ and I - /35/.

KEY: A. Variant I
B. Variant II
C. (ev)

so that the relative yield of the channels $j \geqslant 4$ with excitation of Cameron bands proved to be nearly a smooth function of λ. This is an indication of the reliability of the data in /34/.

There is some disparity between the data in /33/ and in /34/. Therefore we introduce two variants of the distribution of $f_j(\lambda)$ for the 800-1090 Å interval. In variant I it is assumed that $\sum_{j \geqslant 4} f_j(\lambda)$ corresponds to the data in /34/, and $f_3 = 1 - \sum_{j \geqslant 4} f_j(\lambda)$;

in the second variant, f_3 is taken according to the data in [33], and $\sum_{j \geq 4} f_j(\lambda) = 1 - f_3(\lambda)$. It should be noted that the analysis made in [33] of the long-lived state $O(^1S)$ is a complicated problem compared with [34], and the scatter of the resulting data proves to be quite appreciable. Therefore we assume variant I of $f_j(\lambda)$ to be more reliable.

The contribution made by the different channels to the sum $\sum_{j \geq 4} f_j(\lambda)$ can be distinguished, based on the data in [35], in which the absolute excitation cross-sections of the cascade transitions of CO (a', d, e $\rightarrow a^3 \rightarrow X^1\Sigma^+$) were determined. These cross-sections were measured with respect to the fluorescent spectrum induced in the photolysis of CO_2 at individual lines from 764 to 923 Å. The cross-sections measured at 901 and 923 Å are understated, because the detector of fluorescent radiation had a limited spectral sensitivity. If we can take into account the results of [36] (see below, subsection 3.5) and make the appropriate correction, it turns out that at 923 Å the excitation cross-sections of the Asundi bands $_5(a^{13}\Sigma^+ \rightarrow a^3\Pi)$ and the triplet system $\delta_6(d^3\Delta$ [illegible] $\rightarrow a^3\Pi)$ in the sum are equal to the total excitation cross-section of the Cameron bands /14 $\sum_{j \geq 4} \delta_j$ measured in [34]. Thus, for variant I the contribution of the direct dissociative excitation of the Cameron bands, that is, channel No. 4, can be neglected: f_4 (923 Å) = 0. However, for variant II, when λ = 923 Å, the measured cross-sections δ_3, δ_5, and δ_6 in the sum proved to be less than the total absorption cross-section. The difference can be attributed to channel No. 4 (channel No. 7 in this wavelength was not recorded [35]).

The cross-sections at λ = 901 Å for both variants of $f_j(\lambda)$ indicate that other channels with cascade transitions, which were identified with channel No. 7, must also make a contribution to the total excitation of Cameron bands, in addition to channels No. 5 and No. 6.

According to [35], in the 764-835 Å region, the yield of the channels with excitation of fluorescent transitions CO (a', a^2, $e \to a^3\Pi \to \lambda\ ^1\Sigma^+$) represents more than 85 percent with respect to all the dissociative channels. This means that we can neglect all the unrecorded dissociation channels, for example, with the formation of CO ($A^1\Pi$), O(^{3}S, ^{5}S), and so on. When $\lambda \lesssim 900$ Å, we will assume that dissociation proceeds either via channel No. 3 (according to the data in [33] or [34]), or with the formation of CO in the state $e^3\Sigma^-$, and with formation of O -- in the electronically-excited state with the highest possible energy, that is, in channel No. 7 at $\lambda > 809$ Å, No. 8 -- -- at $707 < \lambda < 809$ Å, and channel No. 9 -- at $\lambda < 707$ Å. The short-wave cutoff of this spectral interval, 580 Å, was selected on the condition that the dissociative mechanism of photoabsorption is of low probability (the yield of ionization at 580 Å is in 98-100 percent).

3.5. Let us estimate the role of vibrational excitation of CO during the photodissociation of CO_2, that is, the value of the factor $\phi_j(\lambda)$ in Eq. (15). /15

Direct information on the distribution of the probabilities of excitation of the vibrational levels of CO during the dissociation of CO_2 is available only for fluorescent channels ($j \geqslant 5$) [36] and also for channels with excitation of Cameron bands ($j \geqslant 4$) [34]. In [36], the measurements were conducted at λ = 901 and 923 Å. It turned out that the probability of excitation of the v'-th vibrational channel of the states CO ($a'^3\Sigma^+$) and CO ($d^3\Delta_i$) is quite closely described by the Poisson distribution:

$$\frac{(\Delta E)^{v'} e^{-\Delta E}}{v'!}, \qquad (21)$$

where v' is the vibrational quantum number, and E is an empirical parameter, equal to approximately $(h\nu - E_j)/2(h\nu)_{vib}$

($(h\nu)_{vib}$ is the energy of the vibrational quantum). For the distribution (21), in this case the total amount of vibrational energy of CO formed upon the dissociation of CO_2 is half the excess energy of the photon. Therefore the factor of $\phi_j(\lambda)$ for channels j = 5 and j = 6 at λ = 901 and 923 Å is 1/2.

The distribution of the intensity of Cameron bands measured in /3 4/ can be used for estimating $\phi_4(\lambda)$ from the threshold of channel No. 4 to the next threshold (channel No. 5) in order to cancel out the effect of cascade transitions. At wavelength λ = 1026 Å, the excess energy of the photon represents 3.3 vibrational quanta of CO ($a^3\Pi$), and the measured distribution is best approximated by the Poisson curve with ΔE = 0.75. Therefore, for λ = 1026 Å, for ϕ_4(1026 Å) = I 1 0.75/3.3 = 0.77. /16 The report /3 7/ presents data on the rates of velocities of CO_2 photodissociation products obtained by using a time-of-flight mass spectrometer. In the 1090-1160 Å spectral region, the maximum signal was obtained from particles exhibiting a velocity which corresponded to the transformation in each dissociation act of 0.5 ev into kinetic energy. Dissociation at these wavelengths, according to /3 3/ must occur in channel No. 3 with an 11.6 ev threshold. If the residue of residual photon energy is attributed to the excitation of the internal degrees of freedom of CO, then we can get ϕ_3(1050 - 1160 Å) = = 0.55 ± 0.77.

In a study of the photolysis of CO_2 with a pulsed method in the 1300-1900 Å region /1 5, 3 8/, CO molecules were recorded in the vibrational-excited states v' = 1 and 2. The intensity of the transitions in the absorption spectrum for these levels proved to be approximately ten times less than for the level /symbol omitted/ = 0. Since the energy of the recorded vibrations is approximately one order of magnitude less than the excess energy of the absorbed photons, it can be assumed

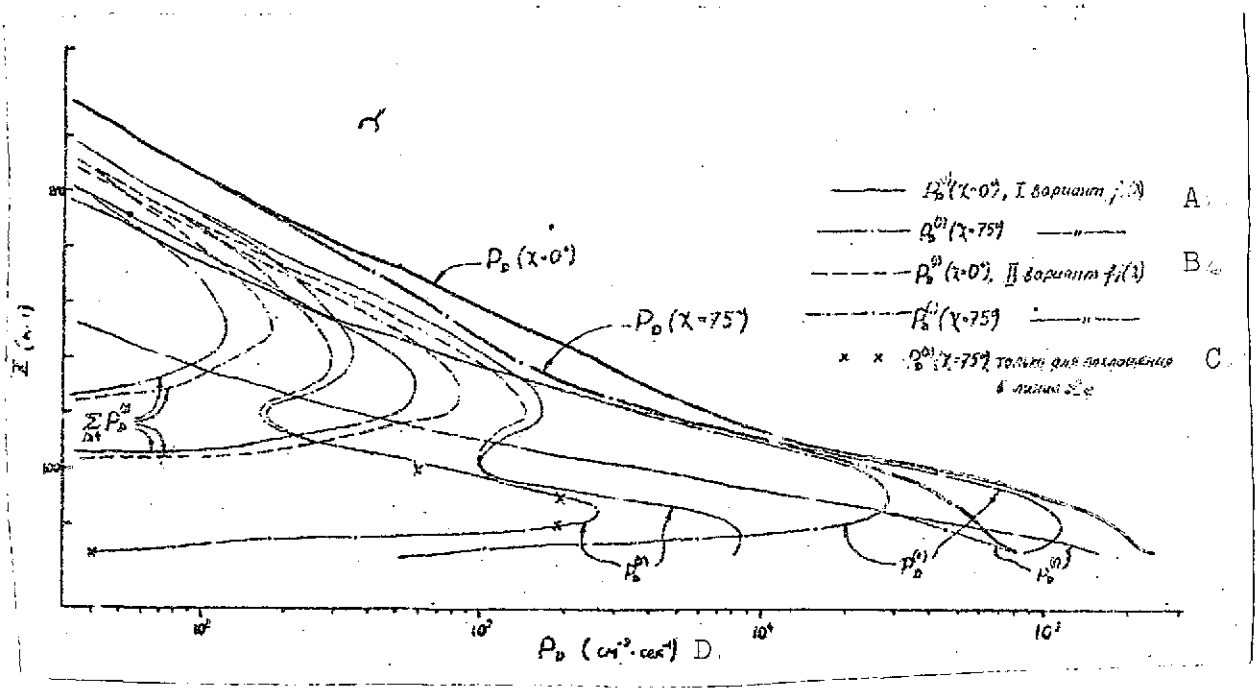

Fig. 2. Distribution of rate of photodissociation, total P_D, and photodissociation with excitation in individual channels ($P_D^{(j)}$) with altitude on Mars.

KEY: A. Variant I of $f_j(\lambda)$
B. Variant II of $f_j(\lambda)$
C. Only for absorption in line λ_a
D. P_D ($cm^{-3} \cdot sec^{-1}$)

that the value $\phi_2(\lambda)$ averaged over the 1300-1500 Å interval is close to unity.

Thus, we see that the amount of information on $\phi_j(\lambda)$ is appreciably less than, for example, on $f_j(\lambda)$. Nonetheless, these data indicate that the actual values of $\phi_j(\lambda)$ for all channels lies in the range 1/2 to 1. We will take as the most probable distribution of ϕ_j the values constant for each channel, presented in Table 2, which are based on an analysis made of the data in [34, 36-38]. We will also consider the two limiting cases with $\phi_j = 1/2$ and $\phi_j = 1$ for all channels. /17

TABLE 2

Channel number	1	2	3	4	5	6	7	8	9
φ_j	1	1	0.66	0.77	0.5	0.5	0.5	0.5	0.5
Reference	-	[38]	[37]	[34]	[36]	[36]	-	-	-

3.6. We note the following concerning the possible conversion of some of the energy of $O(^1D)$ upon deactivation of CO_2 molecules into vibrational degrees of freedom of CO_2 (the factor $\psi_{O(^1D)}$ in Eqs. (17) and (18)). The process of deactivation of $O(^1D) + CO_2 \rightarrow O(^3P) + CO_2$ occurs with a large cross-section, (approximately coinciding with the gas-kinetic cross-section /10/. The higher efficiency indicates the chemical nature of the interaction, with the formation of an intermediate complex CO_3^*. Processes of this type are characterized by a low efficiency of the conversion of energy from the electronic form to the vibrational /39/. (We note that for the terrestrial thermosphere, de-activation of $O(^1D) + N_2 \rightarrow O(^3P) + N_2$ occurs, is shown by quantum-mechanical calculation, nearly without the excitation of the vibrations N_2 /40/.) Therefore in the calculations we will assume $\psi = 1$ for both $O(^1D)$ and $O(^1S)$ (de-activation of $O(^1S)$ in the thermosphere is of low efficiency, and the exact value of the energy transfer characteristics in this process is minor).

4. Results of Calculations and Their Discussion

Let us examine the results of calculating the rate of photodissociation, the heat liberation associated with it, and several emissions arising due to dissociation.

The calculations were made on a computer for Mars in the altitude range 70-300 km and for Venus in the altitude range 100-300 km for several zenithal angles of the Sun: χ = /value not given/, 50, and 75°. /18

The spectral range 580-2274 Å was involved. Owing to the complex functions $\delta(\lambda)$, to approximate it 230 intervals were taken, whose width varied from approximately 1 to 10 Å. Within the limits of each interval, the function $\delta(\lambda)$ is noted to be linear. To find the effect of the structure of cross-sections on the results of calculations, a trial smoothing of $\delta(\lambda)$ was carried out, that is, averaging over an interval of several angstroms about each point of λ. The changes in the results given below do not exceed several percent for all the altitudes. This appears to be a consequence of the fact that we are dealing with characteristics that are integrated over the spectrum.

4.1. The altitude profiles of the photodissociation rate in the thermosphere of Mars in each channel $P_D^{(j)}(z)$ and the total rate of dissociation $E_D(z)$ for the zenithal angles $\chi = 0$ and 75° are presented in Fig. 2. The profiles are indicated for the first variant of the distribution of $f_j(\lambda)$ (more reliable) and for the second variant. Clearly, throughout the range of altitudes considered $P_D(z)$ increases with decrease in altitude (from the calculations given in [11] it follows that this trend of $P_D(z)$ continues down to the surface of Mars). The contribution made by channel No. 1 to the total dissociation is predominant at altitudes less than approximately 75-80 km; from these altitudes to the altitudes of 135-155 km (depending on the χ, the larger altitudes correspond to larger χ), the contribution made by channel No. 2 predominates, and at greater altitudes -- the contribution made by channel No. 3. The maximum dissociation in channel No. 2 lies at the altitude of 80-90 km. The dissociation profile in channel No. 3 has two maxima, where the upper maximum, at 120-140 km, arises due to absorption of photons with $\lambda \lesssim 1150$ Å, where the CO_2 dissociation cross-sections are very large (up to $\delta_D \simeq 10^{-16}$ cm^2), and the second maximum, approximately at 80 km, arises mainly due to absorption of the intense Lyman-alpha solar line of hydrogen

/19

(1216 Å), for which $\delta_D = 8 \cdot 10^{-20}$ cm^2 (the crosses denote $P_D^{(3)}(z)$ only due to Lyman-alpha).

The indeterminacy with respect to $P_D^{(3)}$ due to the difference between the variants I and II of the distribution of $f_3(\lambda)$ becomes marked only above 110 km and is not more than 15 percent. The difference between variants I and II is much greater for the dissociation rate in channels $j \geqslant 4$: the total rate $\sum_{j \geq 4} P_D^{(j)}$ for variant I is one and a half times less than for variant II. The absolute value of the rate $\sum_{j \geq 4} P_D^{(j)}(z)$ has a maximum at the altitude 130-150 km; at this altitude their contribution to the total dissociation rate for the first variant $f_j(\lambda)$ is 25 percent.

The photodissociation rates in different channels in the thermosphere of Venus have approximately the same altitude profiles.

4.2. Fig. 3 gives the values of $\epsilon(N)$ for different zenithal angles also for both planets: Mars and Venus. The calculations were made for the variant I of $f_j(\lambda)$ and for ϕ_j based on Table 2. The scale of N is given at the right; also presented are the altitude scales for the adopted models of the Martian and Venusian thermospheres for $\chi = 0^\circ$. We see that the calculated points $\epsilon(N)$ for the different models lie in the same universal curve over practically the entire thermosphere, with the exception of the region near the exobase. In this region de- /20
activation of $O(^1D)$ owing to the low atmospheric density is replaced by de-excitation, therefore the spectral efficiency ϵ depends not only on the number of particles in the column N, but also on the local concentration n(z).

The maximum of $\epsilon \simeq 0.35$ lies in the lower thermosphere for $N \simeq 10^{17} \div 10^{19}$ cm^{-2}. The decrease in ϵ for larger N is associated with the fact that at the lower altitudes photons

with low excess energy occur (and in this region photoabsorption takes place due to the long-wave spectral region where the cross-section of CO_2 decreases monotonely with wavelength). In the middle and upper thermosphere, ϵ decreases and becomes approximately constant ($\sim$ 0.23) at N = 10^{15} cm^{-2}, which corresponds to an altitude of approximately 200 km for all models. At this level there is an inflection in the profile $\epsilon(N)$ associated with the contribution made by de-excitation of $O(^1D)$.

The function $\epsilon(N)$ is accounted for by the redistribution over altitude of the contribution made by different channels to heat liberation. This can be seen from the altitude profiles of $\epsilon_j(N)$ shown in Fig. 3 for the Martian model when $\epsilon = 0^\circ$. The mean role in the thermosphere is played by channels No. 2 and No. 3. Channel No. 1 becomes appreciable only near the mesopause. The total contribution of channels with $j \geq 4$ to $\epsilon(N)$ is less than 2 percent in the maximum, which greatly reduces the effect of the indeterminacy in $f_j(\lambda)$ for the short-wave range on the value of ϵ. The altitude profiles $\epsilon_j(N)$ for the other zenithal angles and for the Venusian thermosphere differ from those presented, as follows from the profile of $\epsilon(N)$ only in the region above /illegible/ km.

4.3. Altitude profiles of the rate of energy absorption during photodissociation $Q_S(z)$ for $\chi = 0^\circ$ and the rate of heat liberation $Q_{ST}(z)$ for $\chi = 0.50$ and 75° are shown in Fig. 4 for the thermosphere of Mars (variant I of $f_j(\lambda)$, ϕ_j based on Table 2). Here also is presented, for comparison, the profile of the rate of energy absorption during photo-ionization Q_S^u for $\chi = 0^\circ$ (calculated analogously to Q_S, but with a smaller energy resolution: in the 30-902 Å range, $F_\infty(\lambda)$, $\delta(\lambda)$, and the ionization cross-sections $\delta_u(\lambda)$ were averaged over ten spectral intervals). A comparison of Q_S and Q_S^u shows that in the upper thermosphere, beginning with the altitude of 130 km

/21

Q_S^u exceeded Q_S by 2-2.5 times; at the altitude of 115 km, their values are comparable: at lower altitudes Q_S^u very rapidly drops off, while Q_S continues to rise.

Q_{ST} reaches a maximum at 70-80 km, where here for $\chi = 0^\circ$ $Q_{ST} = 10^{-6}$ erg/cm^3·sec, and for $\chi = 75^\circ$ $Q_{ST} = 2 \cdot 10^{-7}$ erg/cm^2·sec.

The altitude profiles of energy absorption $q_S(z)$ and heat liberation per unit mass $q_{ST}(z)$ in the thermosphere of Mars for $\chi = 0^\circ$ are shown in Fig. 5. The heavy line denotes the most probable profile of $q_{ST}^b(z)$ (variant I of $f_j(\lambda)$, and ϕ_j according to Table). Clearly, while q_S at the altitudes of 200 km and higher remains constant ($\sim 10^5$ erg/g·sec), the value of q_{ST} reaches a maximum at 170-200 km ($2 \cdot 10^4$ erg/g·sec) and then begins to decrease with increase in altitude owing to the de-excitation of $O(^1D)$.

In the same figure it can be seen the indeterminacies that are caused by the various assumptions. For variant I of $f_j(\lambda)$ and the limiting values of the factor of $\phi_j = 1/2$ and $\phi_j = 1$, the profiles of $q_{ST}(z)$ differ from $q_{ST}^b(z)$ in the upper thermosphere (up to 200 km) by not more than $\pm$ 13 percent. In the lower thermosphere, the profile of $q_{ST}^b(z)$ coincides with the profile for $\phi_j = 1$ and differ from the profile for $\phi_j = 1/2$ by $\pm$ 20 percent. /22

The indeterminacy due to $f_j(\lambda)$ is less than due to ϕ_j. It is absent at the lower altitudes, while it does not exceed 10 percent at the higher altitudes.

In Fig. 5, circles denote the values of $q_{ST}(z)$ calculated by using the data in [26] on the decrease in the quantum yield of the photodissociation products of CO_2 in the spectral region of channel No. 2. In the remaining region of the spectrum, the variant I of $f_j(\lambda)$ was adopted, and q_j was taken according to Table 2. The value of $q_{ST}(z)$ at the altitude of 100 km proved

to be less than q_{ST}, by 25 percent. The difference is appreciable, but still before confirmation of the results of the experiment in [26], the difference must be approached cautiously.

We note that all these indeterminacies must lead to the same errors also in the calculation of Q_{ST} and ϵ. Therefore the analysis made, as well as the small contribution to heat liberation of shortwave channels, suggest the conclusion that the assumptions that we made in constructing the most probable distribution of $f_j(\lambda)$ and ϕ_j (linear approximation of $f_j(\lambda)$, constancy of ϕ_j for each channel, restriction of the number of channels, and cutoff on the short-wavelength side) are admissible. If we cancel out the errors associated with the model, by converting to the universal dependences on N, then only the errors associated with the indeterminacies in the cross-sections of $\delta(\lambda)$ and in the flux $F_\infty(\lambda)$ remain the most substantial for the calculation of the desired quantities. /23
Here, it should be noted that the most exact of all the functions obtained is $\epsilon(N)$, since the arbitrary cofactor in front of $F_\infty(\lambda)$ does not change the value of $\epsilon(N)$. For this reason, $\epsilon(N)$ depends weakly on solar activity.

4.4. The universal functions $q_{ST}(N)$, $P_D(N)$, and $Q_{ST}(N/P_D(N))$ are shown in Fig. 6. The scales of the values of P_D and Q_{ST} for Mars are shifted to the right relative to the scales for Venus, by the dilution factor $(R_\sigma/R_\varphi)^2 = 4.45$. The calculation was based on variant I of $f_j(\lambda)$ and δ_j taken according to Table 2, the model used was that of the Martian thermosphere, and $\chi = 0^\circ$ (the other models yield differing values only when $z > 200$ km).

The presence of two ranges is a common feature of the functions $P_D(N)$ and $Q_{ST}(N)$ shown in the figure: the upper limit, when $N \lesssim 10^{17}$ cm^{-2} (that is, $z \gtrsim 115$ km on Mars and $z \gtrsim 140$ km on Venus), and the other, the lower limit, when

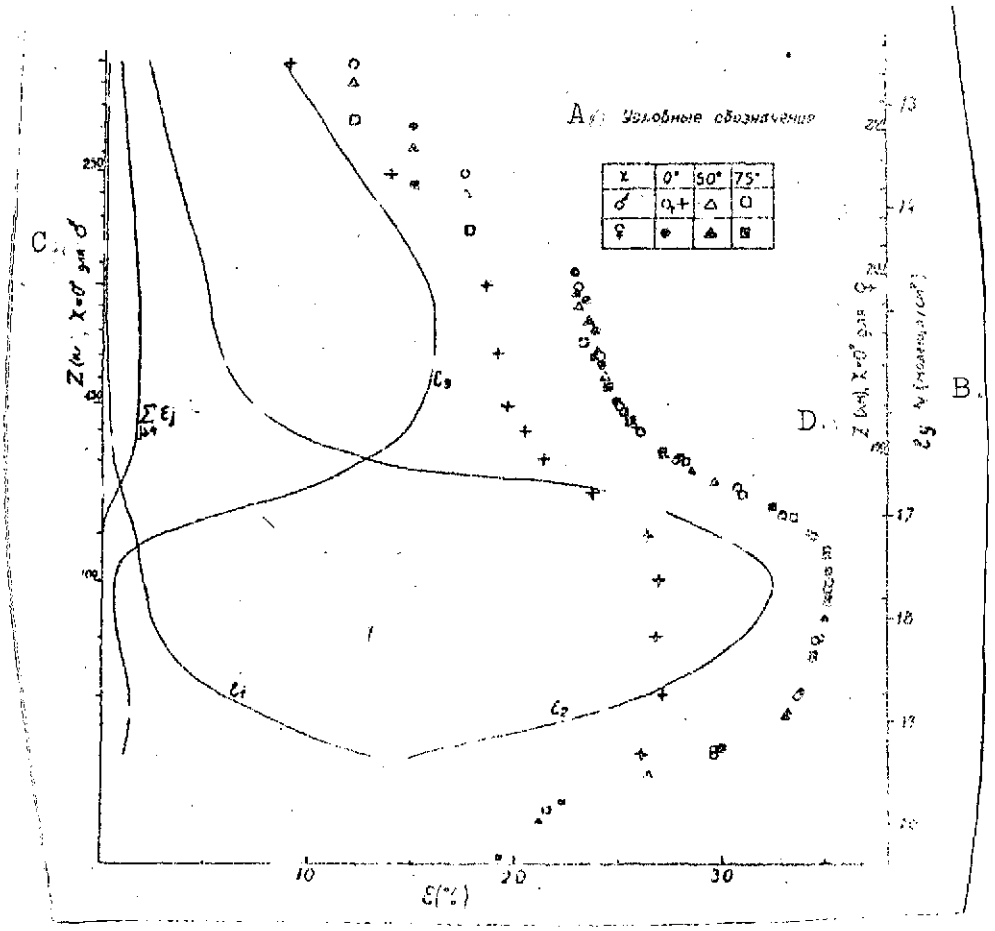

Fig. 3. Dependence of effectiveness of heat liberation ϵ and efficiencies of heat liberation in individual channels ϵ_j on the number of molecules in the photon paths N and on the altitude on Mars and on Venus.

KEY: A. Legend
B. N (molecule/cm^2)
C. Z (km) $\chi = 0^\circ$ for ♂
D. Z (km) $\chi = 0^\circ$ for ♀

$N \geqslant 10^{17}$ cm^{-2}, in each of which the slow change of these functions of N in the upper part of the range characteristic of an optically thin layer is replaced by the rapid change in the lower part of the range. This is associated with the absorption of various spectral intervals at different altitudes as a function of $\delta(\lambda)$. This characteristic is suitable for approximation of these functions.

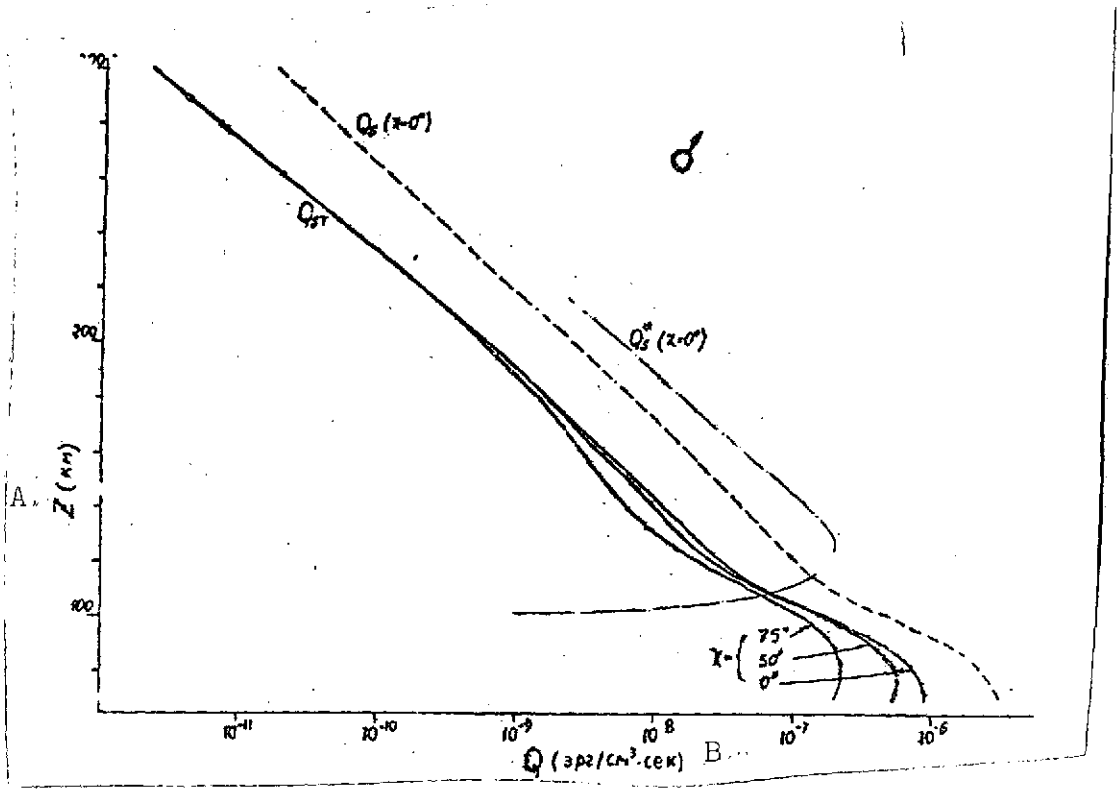

Fig. 4. Dependence of bulk absorption of energy Q_S due to photodissociation, Q_S^u due to photo-ionization, and rate of heat liberation Q_{ST} on altitude for Mars.

KEY: A. z (km)
B. Q (erg/cm^3·sec)

A comparison of our values $P_D^{(j)}$ with the data in [1] shows that the rate of photodissociation in several channels, according to our calculations, is approximately twice as high as according to [1]. Obviously, this is accounted for by the reduction, by twofold, in [1] of the flux $F_\infty(\lambda)$.

The quantity Q_{ST}/P_D shown in Fig. 6 characterizes the amount of energy which on the average is given off as heat as the result of a single act of dissociation. It is found that in most of the thermosphere, with the exception of $z \gtrsim 200$ km, each photodissociation act leads to the release of about 3 ev of heat. /24

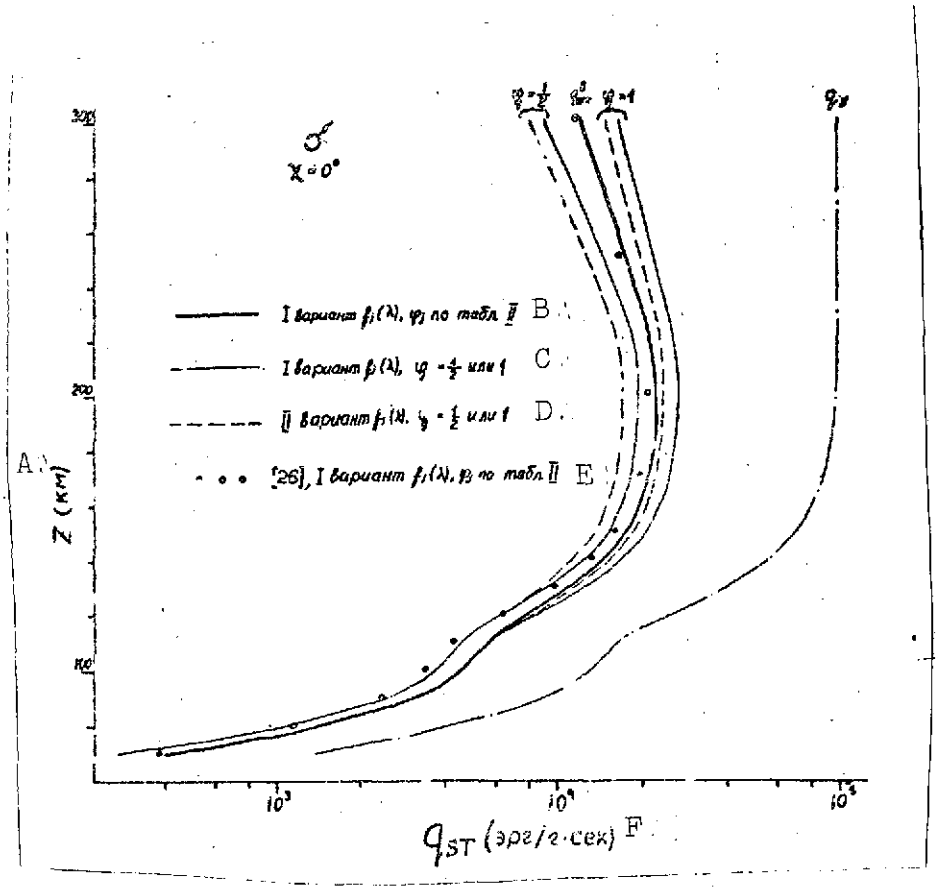

Fig. 5. Dependence of specific absorption of energy Q_S and rate of heat liberation Q_{ST} on altitude for Mars at the zenithal angle $\chi = 0^{\circ}$.

KEY: A. Z (km)
B. Variant I of $f_j(\lambda)$, δ_j based on Table 2.
C. Variant I of $f_j(\lambda)$, δ_j = 1/2 or 1
D. Variant II of $f_j(\lambda)$, δ_j = 1/2 or 1
E. /26/, Variant I of $f_j(\lambda)$, δ_j based on Table 2
F. Q_{ST} (erg/g·sec)

4.5. The calculation made of the photodissociation rate makes it possible to obtain the intensity of the emissions induced thereby. The following emissions were calculated: $O(^1S \rightarrow {}^1D)$, λ = 5577 Å; $O(^1S \rightarrow {}^3P)$, λ = 2972 Å; and $O(^1D \rightarrow {}^3P)$,

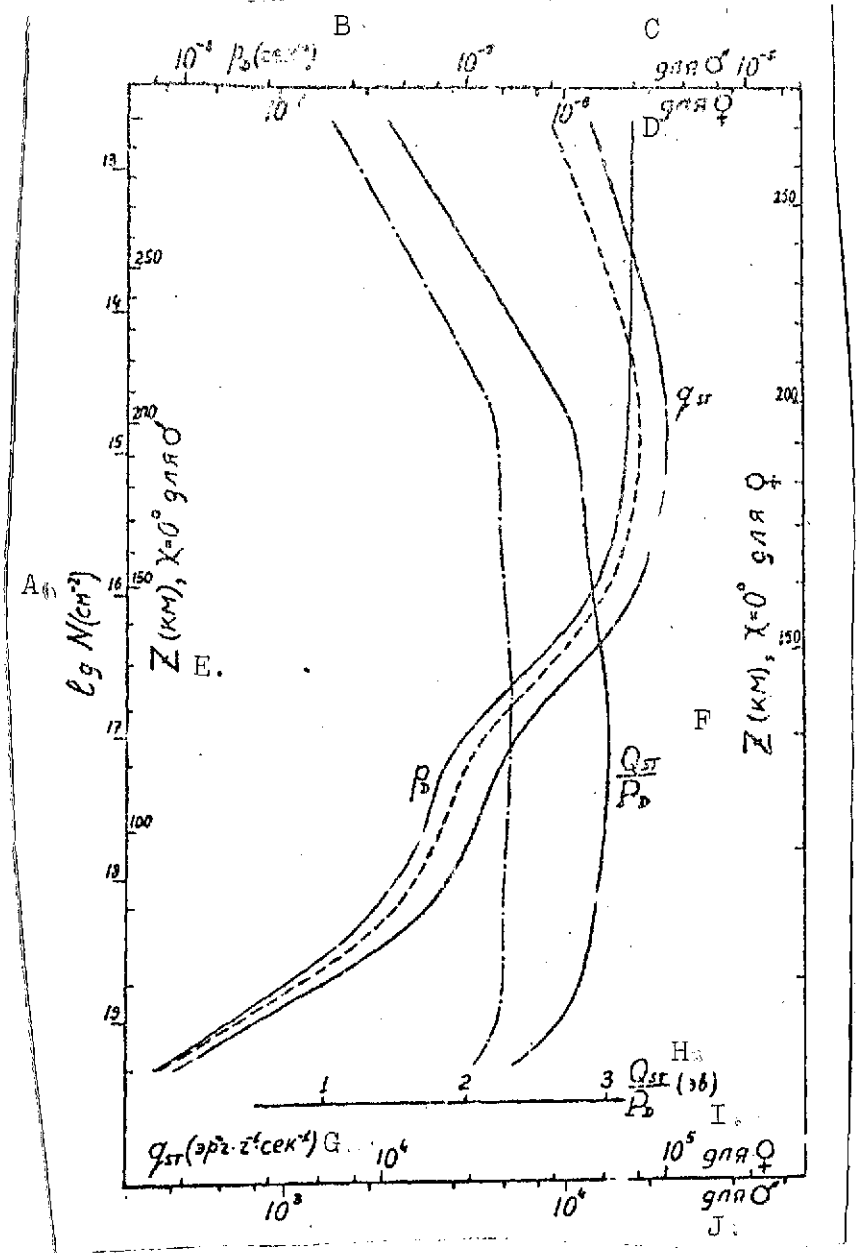

Fig. 6. Dependence of rate of photodissociation per particle P_D, specific rate of heat liberation Q_{ST}, and mean energy per active photodissociation Q_{ST}/P_D on number of molecules in photon path N and on the altitude on Mars and Venus

KEY: A. lg N (cm^{-2})
B. P_D (sec^{-1})
C. For ♂
D. For ♀
E. Z (km), $\chi = 0^\circ$ for ♂
F. Z (km), $\chi = 0^\circ$ for ♀
G. Q_{ST} ($erg \cdot g^{-1} \cdot sec^{-1}$)
H. Q_{ST}/P_D (ev)
I. For ♀
J. For ♂

λ = 6300 Å. The formulas for calculating the bulk radiance (in units of photon/$cm^2 \cdot sec$) are of the form

$$R(5577) = P_{20}^{(3)} / \{1 + (A_{O(^1S \to {}^3P)} + K_{O(^1S)} n) / A_{O(^1S \to {}^1D)}\},$$

$$R(6300) = \{P_0^{(2)} + P_{20}^{(3)} / (1 + [A_{O(^1S \to {}^3P)} + K_{O(^1S)} n] / A_{O(^1S \to {}^1D)})\} / (1 + K_{O(^1D)} n / A_{O(^1D \to {}^3P)}), \quad (22)$$

$$R(2972) = P_{20}^{(3)} / \{1 + (A_{O(^1S \to {}^1D)} + K_{O(^1S)} n) / A_{O(^1S \to {}^3P)}\}.$$

Here we do not take into account the formation of excited O in channels No. 8 and No. 9, which cannot lead to an appreciable error. Since in the upper atmosphere dea activation of CO ($a^3\Pi$) is not efficient, the bulk radiance of emission in the Cameron bands obviously is equal to the sum $\sum_{j \geq 4} P_D^{(j)}$ of the photodissociation rate over all channels, leading

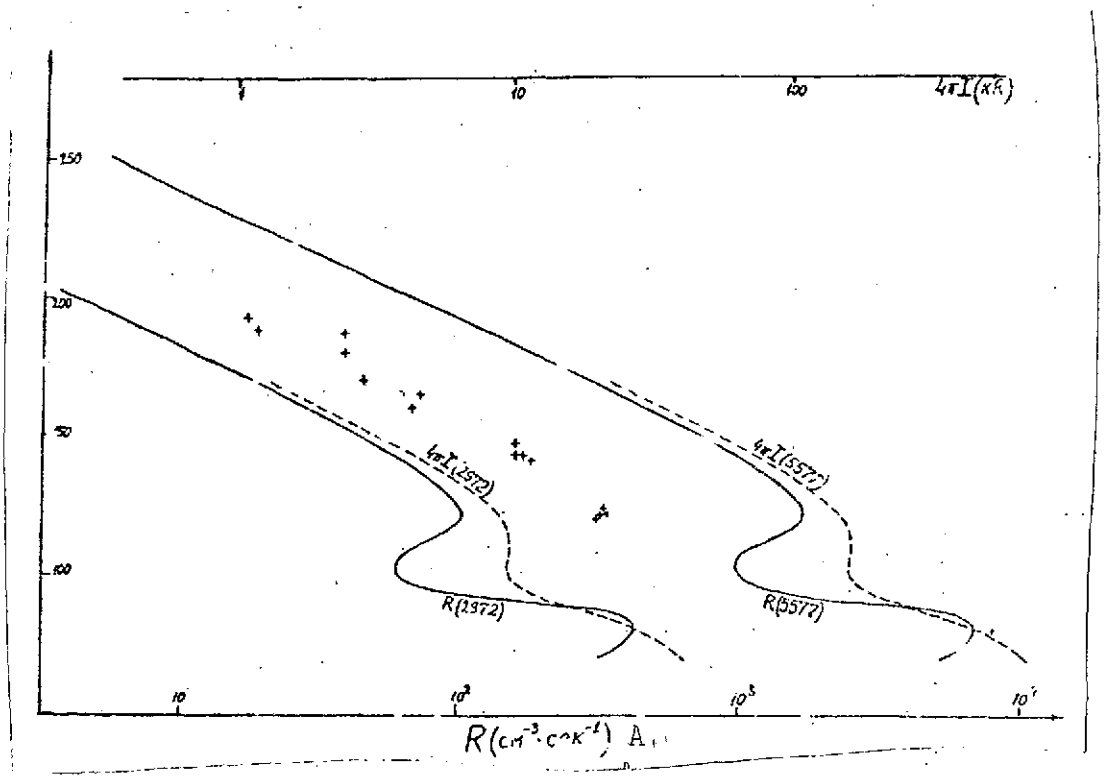

Fig. 7. Bulk radiance R and limbic intensity $4\pi I$ for the emissions OI (2972 Å) and OI (5577 Å) calculated for the Martian thermosphere (variant I of $f_j(\lambda)$, $\chi = 0^\circ$). The solid lines denote R, the dashed lines denotes $4\pi I$, + denotes the experimental data of measurements of $4\pi I$ for OI (2972 Å) [43]. KEY: A. R ($cm^{-3} \cdot sec^{-1}$)

by direct or cascade transitions to the formation of CO ($a^3\Pi$). This value is shown in Fig. 2. Fig. 7 gives R (5577) and R (2972 Å) for the Martian thermosphere, $\chi = 0^\circ$, variant I of $f_j(\lambda)$. Since the de-activation of $O(^1S)$ is noticeable only near the mesopause, in most of the thermosphere R (5577 Å) to a precision of the constant factor 0.94 coincides with $P_D^{(3)}$; the mission OI (2972 Å) is 16.4 times weaker [42]. As noted above, the de-excitation of $O(^1D)$ begins only at $Z \geqslant 200$ km, /25 therefore R (6300 Å) all the way up to this level proves to be very small, increasing slowly from tenths of a photon/$cm^3 \cdot sec$ at low altitudes to several units -- at higher altitude.

Let us compare our calculated data for emissions with the experimental measurements of the UV-glow of the upper Martian atmosphere made on the Mariner 6 and 7 spacecraft /43/. Among the measured emissions, OI 92972 Å) was recorded. For comparison with the experiment, we must convert from the bulk radiance R to the limbic intensity of emission, which is directly measured by

$$4\pi I = \int R(\omega) ds. \qquad (23)$$

Integration here is carried out along the line of sight. Fig. 7 gives R and 4 I for OI (2972 Å) and OI (5577 Å) calculated for the Martian thermosphere, for $\chi = 0^\circ$. Here also are presented the experimentally measured limbic intensities OI (2972 Å) (conditions of measurements corresponding to the zenithal angles from 0 to 44°). We see that the profiles of OI 92972 Å) in the thermosphere have a characteristic knee associated with the upper maximum of the rate of formation of $O(^1S)$ (see curve $P_D^{(3)}(z)$ in Fig. 2. The lower maximum must lead to a knee in the profile now in the region of the mesosphere (possibly owing to greater density it will be masked by Rayleigh scattering). The intensity of the altitudes 100-120 km proved to be 10 kR. Since the intensity at the altitude 120 km measured on Mariner 6 and 7 was 21 kR, there must be an additional emission source. This cannot be photoelectronic excitation, since according to /44/, photoelectrons /26
make a contribution to the emission OI (2972 Å) that is one order smaller than photodissociation. The dissociative recombination of the ions CO_2^+ or O_2^+ with excitation of $O(^1S)$ can be this source.

5. Summary

Photodissociation in the thermospheres of Mars and Venus occurs in several channels of dissociation with excitation, whose relative role varies with change in altitude.

The total photodissociation rate P_D and the associated heat liberation Q_{ST}, with decrease in altitude, increases all the way to the mesosphere. In the lower part of the thermosphere heat liberation due to photodissociation is greater than due to photo-ionization, and less -- in the upper thermosphere.

The efficiency of heat liberation $\epsilon(Z)$ varies from a maximum of 0.35 in the lower thermosphere to 0.23 in the upper thermosphere (approximately at 200 km), and even less, near the exobase.

The universal characteristics $P_D(N)$, $q_{ST}(N)$, and $\epsilon(N)$ obtained do not depend on the adopted model and the zenithal angle of the Sun throughout the entire thermosphere, with the exception of the region around the exobase.

Addendum: It is experimentally shown in [4,5] that in the deactivation of the level $O(^4D)$ by CO and N_2 molecules, 30-40 percent of the energy is converted into vibrational degrees of freedom. Possibly, the same also occurs in CO_2, after which this fraction of the energy is de-excited. To take into account this indeterminacy, in addition to calculations with $\phi_o(^1D) = 1$, calculations were conducted with $\phi_o(^1D) = 0.6$. As a result of these calculations, ϵ and q_{ST} were reduced by approximately 20 percent. The results for ϵ are shown in Fig. 3 by crosses and in Fig. 6 -- by a dashed line for q_{ST}, and by a dash-dot line for Q_{ST}/P_D.

REFERENCES

1. McElroy, M. B., and McConnell, J. C., J. Atmos. Sci. 28, 879 (1971).

2. Barth, C. A. et al., Icarus 17, 457 (1972).

3. Shimizu, M., Space Research 12, 293 (1972).

4. Dickinson, R. E., J. Atmos. Sci. 28, 1358 (1971).

5. Dickinson, R. E., and Ridley, E. C., J. Atmos. Sci. 29, 1557 (1972).

6. Whitten, R. C., and Sims, J. S., Planet. Space Sci. 21, 1333 (1973).

7. Henry, R. J. W., and McElroy, M. B., in: The atmospheres of Venus and Mars, 1968, p. 251.

8. Stewart, A. J., Geophys. Res. 77, 54 (1972).

9. Pravilov, A. M., and Vilesov, F. I., in the collection: Uspekhi fotoniki 3, p. 3 (1973).

10. Herdner, Husain, Nature, Phys. Sci. 241, 10 (1973).

11. Young, R. A., and Black, G. J., Chem. Phys. 44, 3741 (1966).

12. Izakov, M. N., Geomagn. i aeronomiya 10, 283 (1970).

13. Izakov, M. N. and Morozov, S. I., Geomagn. i aeronomiya 10, 630 (1970).

14. Goody, R. M., Atmosfernaya radiatsiya /Atmospheric Radiation/, Moscow, Mir Press, 1966.

15. Barat, F. Rapp. /sic/ SEA, NR-3865, 1970.

16. Stupochenko, Ye. V., Losev, S. A., and Osipov, A. I., Relaksatsionnyye protsessy v udarnykh volnakh /Relaxation Processes in Shock Waves/, Moscow, Nauka Press, 1965.

17. Taylor, R. L., and Bitterman, S., Rev. Modern Phys. 41, 26 (1969).

18. Slanger, T. G., and Black, G. J., J. Chem. Phys 53, 3722 (1970).

19. Hogan, J. S., and Stewart, R. W., J. Atmos. Sci. 26, 332 (1969).

20. McElroy, M. B., Ann. Geophys. 26, 543 (1970).

21. Moroz, /illegible/ I., Uspekhi fiz. nauk 104, 255 (1971).

22. Hinteregger, R. E., Ann. Geophys. 26, 517 (1970).

23. Ackerman, M., Mesospheric models and related experiments, Dordrecht-Holland, D. Reidel Pub. Co., 1971, p. 149.

24. Nakata, R. S. et al., Science of Light, Tokyo 14, 54 (1965).

25. Ogawa, M., J. Chem. Phys. 54, 2550 (1971).

26. Inn, E. C. Y., and Heimerl, J. M., J. Atm. Sci. 28, 838 (1971).

27. Clark, J. D., and Noxon, J. F., J. Geophys. Res. 75, 7307 (1970).

28. Baulen, D. C., and Breckenridge, W. H., Trans. Farad. Soc. 62, 2768 (1966).

29. Slanger, T. G., and Black, G., J. Chem. Phys. 54, 1889 (1971).

30. Mahan, B. H., J. Chem. Phys. 33, 959 (1960).

31. Sun, H., Weissler, G. L., J. Chem. Phys. 23, 1625 (1955).

32. Inn, E. C. Y., J. Geophys. Res. 77, 1991 (1972).

33. Lawrence, G. M., J. Chem. Phys. 57, 5616 (1972).

34. Lawrence, G. M., J. Chem. Phys. 58, (1973).

35. Judge, D. L., and Lee, L. C., J. Chem. Phys. 57, 104 (1972).

36. Lee, L. C., and Judge, D. L., Canad. J. Phys. 51, 378 (1973).

37. Welge, Gilpen, J. Chem. Phys. 54, 4224 (1971).

38. Clerc, M., and Barat /initial missing/, J. Chem. Phys 54, 107 (1967).

39. Kallir, A., and Lambert, J., in the collection: Vozbuzhdennyye chastitsy v khimicheskoy kinetike /Excited Particles in Chemical Kinetics/, Moscow, Mir Press, 1973.

40. Fisher, E. R., and Bauer, E. J., J. Chem. Phys 57, 1966 (1972).

41. McElroy, M. B., and Hunten, D. M., J. Geophys. Res. 75, 1188 (1970).

42. Garstag, R. H., Month. Nat. Roy. Astron. Soc. 111, 115 (1951).

43. Barth, C. A. et al., J. Geophys. Res. 76, 2213 (1971).

44. McConnell, J. C., and McElroy, M. B., J. Geophys. Res. 75, 7290 (1970).

45. Slanger, T. G., and Black, G. I., J. Chem. Phys. 60, 2 (1974).